S. Supporting information: Methods and materials

The MATLAB code used for data analysis, raw data, simulations, graphs, photos and videos of the experiments is available from the following website: Raindrop measurement with event camera.

This supplementary material has the following sections:

- S.1 provides details on the Dynamic Vision Sensor (**DVS**) event camera.
- S.2 describes our Hard Disk Droplet Generator (**HDDG**) and Intravenous Dripper Droplet Generator (**IVDG**).
  - S.2.1 details our droplet needle.
  - S.2.2 details construction of the HDDG.
  - S.2.3 provides additional useful methodology for testing the stability of the HDDG
  - S.2.4 describes unsuccessful attempts to develop hydrophobic coatings to reduce the IVDG droplet size.
- S.3 details our experimental setups.
- S.4 describes our experiments and the methods we used to measure droplets and estimate uncertainty, in particular
  - S.4.2 details our error analysis.
  - S.4.3 explains how we optimized our droplet illumination.
  - Secs. S.4.7, S.4.4, and S.4.5 explain our calibration of the optical magnification of the camera M, angle α, and droplet fall height.
  - S.4.6 explains how we measured the droplet diameter and speed in the image plane
  - S.4.10 provides formulas to compute the physical diameter and speed from the image plane measurements.
  - S.4.11 describes how we measure droplet flow rate for ground-truth droplet size estimates.
  - S.4.12 further details our ground truth (**GT**) measurement of droplet mass.
- S.5 explains our model of the droplet speed versus fall height and droplet diameter, which we used to obtain our GT speed from mass and to ensure that droplets fell at close to terminal speed.

S.1. Dynamic vision sensor event camera

The Dynamic Vision Sensor Disdrometer (**DVSD**) uses a DVS event camera. Fig. S1 shows the DVS pixel circuit. Its design is based on the DVS (Lichtsteiner, Posch, and Delbruck 2008) and the Dynamic and Active Pixel Vision Sensor (**DAVIS**) (Brandli et al. 2014) with improvements described in Taverni et al. (2018). It was developed by the Delbruck lab and is sold by inivation.com as the DAVIS346 camera. For the DVS brightness change events used for drop measurement, the logarithmic photoreceptor (**A**) drives a change detector (**B**) that generates the ON and OFF events (**D**). Pixel photoreceptors continuously transduce the photocurrent I produced by the photodiode (**PD**) to a logarithmic voltage V_p, resulting in a dynamic range of more than 120 dB. This logarithmic voltage (called *brightness* here) is buffered by a unity-gain source follower to the voltage V_sf, which is stored in a capacitor C_DVS inside individual pixels, where it is continuously compared to the new input. If the change V_d in log intensity exceeds a critical event threshold, an ON or OFF event is generated, representing an increase or decrease of brightness. The event thresholds θ_on and θ_off are nominally identical for the entire array. The time interval between individual events is inversely proportional to the derivative of the brightness. When an event is generated, the pixel's location and the sign of the brightness change are immediately transmitted to an arbiter circuit surrounding the pixel array, then off-chip as a pixel address, and a timestamp is assigned to individual events. The arbiter circuit then resets the pixel's change detector so that the pixel can generate a new event. Events can be read out at up to rates of about 10 MHz. The quiescent (noise) event rate is a few kHz. Events are transmitted from the DAVIS chip to a host computer over Universal Serial Bus (**USB**). The host software records the data and allows playback in slow motion. In addition to the DVS circuit the DAVIS346 also has a circuit for conventional intensity frame recordings called the Active Pixel Sensor (**APS**) circuit (Fig. S1C), which was useful for lens calibration and focusing.

S.2. Droplet generation

Figs. 1D and S2 illustrate our HDDG and Fig. S3 shows photos of the HDDG setup. Our HDDG is based on previous work by Kosch and Ashgriz (2015), who utilized a computer hard disk arm as an actuator. They used a high-frequency buzz to create ripples in a steady stream of water emitted by a stiff glass needle, which would break up into small droplets. Our HDDG uses a soft and flexible plastic needle, which, if properly combined with a controlled stream of water, reliably creates a single droplet at each end of an oscillation, resulting in two droplet streams, one of which we measured.

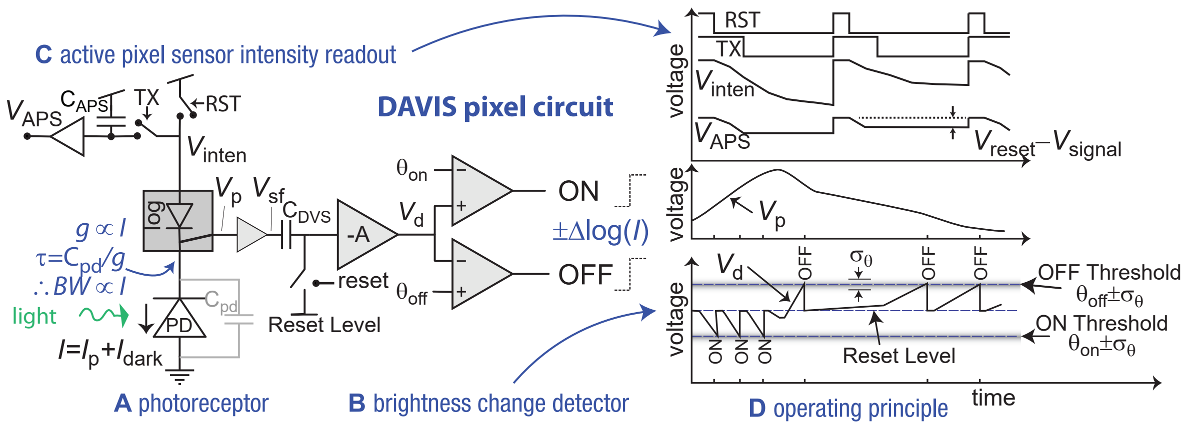

Figure S1: DAVIS pixel circuit and operating principle. The sensor generates asynchronous brightness change ON and OFF DVS events and APS intensity samples, which we do not use for disdrometry, but are helpful for calibration and focusing.

S.2.1. HDDG droplet needle

To make the droplet needle, we used a microloader microcapillary tip[a] This soft plastic needle tubing protrudes from its integrated feeder expansion. The peristalitc pump tubing[b] is plugged into this microloader. The needle is threaded through a hole drilled through the hard disk drive (**HDD**) actuator arm so that the needle protrudes from the arm by 2 cm–4 cm, and we can control the length of the protruding needle to adjust its resonance frequency to match the driving frequency. That way, we can use a smaller driving voltage and current for the HDD driver coils. The needle is fixed to an elevated platform with a conical interference fit between the needle and a black plastic tube glued to that platform (see Fig. S3 C and D). The HDD arm is actuated with an audio power amplifier driven by sinusoidal waveforms generated by an audio wave generating program (www.szynalski.com/tone-generator). The arm is coupled to the needle by threading the needle through one-sided adhesive tape which is applied over the hole in the arm. We used amplitudes from 3 Vpp–10 Vpp and frequencies from 60 Hz–220 Hz. By adjusting the flow rate and oscillation frequency, we can arrive at a combination of settings where nearly on every oscillation, a single droplet is flung from the needle tip at each end of the oscillation. Since the flow rate and frequency are constant, the droplet sizes are also constant.

To create large droplets, we used an IVDG assembled from a standard IV dripper and a needle tip intended for glue dispensers[c]. The diameter of the needle has only a weak influence on the droplet size, which is mainly determined by the surface tension of water adhering to the needle; at low flow rates, when the droplet mass grows large enough, it breaks free from the needle. We adjusted the IV flow to produce a regular series of droplets.

S.2.2. Construction of HDDG droplet generator

Fig. S2 sketches the HDDG construction. We used an old 250GB 3.5” hard disk drive that we disassembled to expose the platter head actuator arm. The copper wires have two functions: first, to power the HDD coils and second, to act like springs to keep the HDD arm close to the middle of the two magnets, which is the best operating point for the arm. To construct the needle driver, we follow these steps:

1. The upper end of the plastic needle was frictionally held in place (see black tube).
2. Two nuts and a bolt (Fig. S3D) could adjust the protruding length of the needle to match the resonance frequency of the needle with the HDD frequency to maximize the amplitude of the oscillation and, therefore, the efficiency.
3. The lower end of the plastic needle was guided through a tiny hole in a piece of sticky tape. The tape was attached to the end of the HDD arm.
4. The needle was connected to the water tube from the pump. This connection must be tight to prevent water leakage and to prevent the needle from twisting.
5. Since the needle has some inherent curvature, we twisted it with our fingers until the inherent curvature was perpendicular to the oscillation direction.

[a] OD 0.3 mm Eppendorf 20 ul microcapillary pipette; Merck Catalog No. 930001007
[b] OD 3.5 mm Tygon® S3™E-3603, Saint-Gobain Performance Plastics; Tygon tubing website
[c] ID 0.2 mm, OD 0.4 mm, part VD90.0032 https://www.martin-smt.de

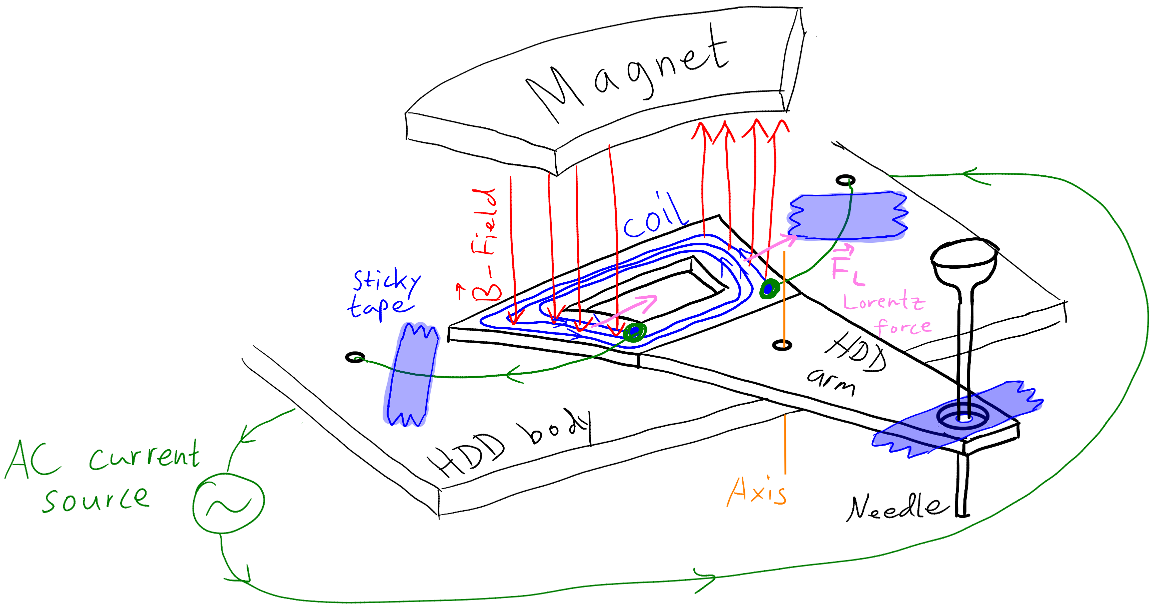

Figure S2: Sketch of HDDG. The red B-vector is the induced magnetic field by the coil and alternates its direction from up to down. When it points up, it is attracted to upwards pointing yellow B-vectors from the static magnet. Two sticky tapes and two green wires hold the HDD arm in place in a spring-like manner. This attachment ensures that the coil is centered between the two opposite poles of the metal piece. Without the sticky tapes, we observed that the arm drifts to one side and does not function properly anymore.

S.2.3. Testing the stability of the hard disk drop generator with a strobe light

It can be observed in our sample recording video that the HDDG droplet jet always changed direction a bit. It seemed that the jet moved in "waves" and "cycles". So we had to be patient and lucky that the jet landed in the DVS measurement area. This is what we meant by "unstable drop generation by HDDG" in Sec. 4. There are probably several effects that caused this behavior, *i.e.*, irregular water flow from the pump, loosely attached needle (so that it can rotate and tilt slightly) and air currents. We believe that air currents only played a minor role and that the most likely culprit is the circular hole in the HDD arm that couples it with the needle (Fig. S3E).

Under our lighting and with HDDG drop generation frequencies above 20 Hz, any errors with the HDDG drop release are too fast to be seen with the naked eye. Thus, to test the HDDG drop release, we used a custom-built strobe light to illuminate the oscillating needle. For the initial experiments, the goal was to create one drop per cycle, which meant that the drop stream was one-sided. For higher frequencies, it was impossible to tell if a drop is released every one or every two cycles. We built an Arduino-driven LED strobe light to check the drop creation frequency using the principle of aliasing. We set the strobe light frequency to the same as the desired drop creation frequency for two seconds, and for another two seconds, the strobe frequency was half of the desired drop creation frequency. If the distance between successive droplets (see Fig. S3F) changes between the droplets when illuminated with the two different strobing frequencies (i.e. distance doubles when the strobe light is flashing at half the desired drop creation frequency), only one drop is released every second cycle. If the distance between the droplets stays the same, one droplet is released per cycle, which is desired.

S.2.4. Testing different hydrophobic coatings for the IVDG

Using a basic IVDG generates different drop sizes that are created depending on the needle size, water surface tension and needle materials. The bigger the needle orifice, the larger the drops. However, this is limited at some point since small drops stick to the needle due to attraction between water and needle tip. The needle surface can be made water repellent by applying a hydrophobic coating. This is rather difficult to do, since the needle orifice is often too small for this coating to fully enter, and the coating is also washed away after a few minutes by the water itself. Also, we did some tests with soap to lower the surface tension of the water. The results did not look promising, which prompted us to develop a droplet generator that can reliably generate drops of the desired size.

S.3. Experimental setups

The HDDG experiment is shown in Fig. S3, while images of the IVDG experiment can be found in Fig. S4.

Fig. S5 illustrates the HDDG setup (left side) and IVDG setup, from a side view perspective. The HDDG setup is additionally shown from a top view in Fig. S5 (bottom left corner) .

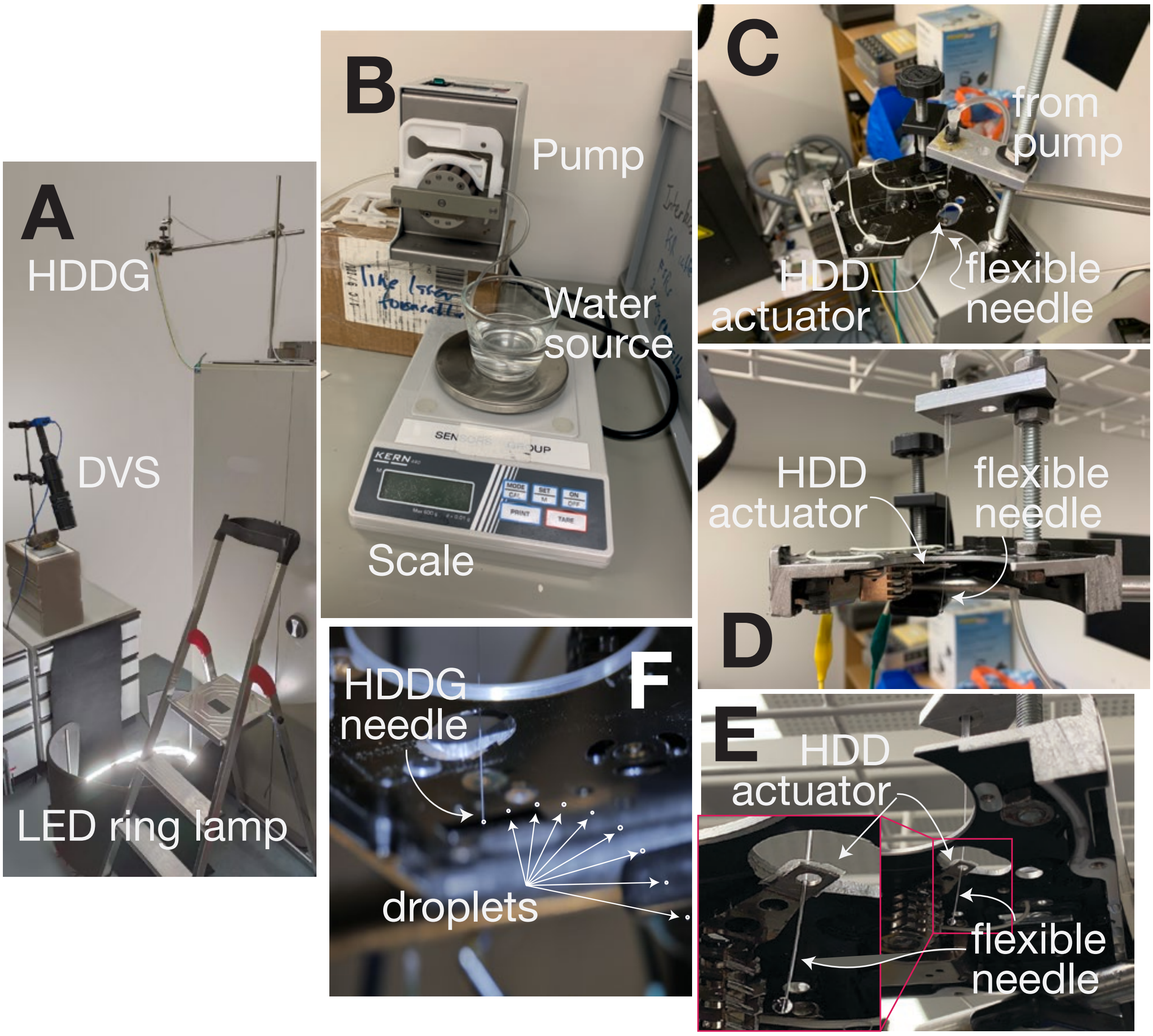

Figure S3: Pictures of the HDDG experimental setup. **A**: Overview of the whole HDDG setup. **B**: Peristaltic pump, scale and water tank. **C, D, E**: HDDG drop generator from three different perspectives. **F**: Stream of droplets created by the HDDG.

S.4. Experiments

375 The objective of the experiments was to measure the diameter and velocity of droplets with a DVS with droplets falling close to their terminal speed, and to compare these measurements with their corresponding GT. Two experiments were conducted with different setups to optimize droplet creation for two different drop size categories, which are further explained in the following two paragraphs. Both experiments used the exact same DVS camera and measurement principles (described in S.4.10). Both lenses were set at their minimum focusing
380 distance. The working distance was then reduced further to about 50 cm using lens spacers. The DVS was a DAVIS (model: DAVIS346), designed by the Delbruck group and manufactured by iniVation. It has a resolution of 346×260 pixels and a pixel array size of $8 \times 6\,\mathrm{mm}^2$ (Brandli et al. 2014; Taverni et al. 2018). Pixels have a pitch of $18.5\,\mu$m. Table S1 compares both experimental setups with further details. Both droplet generation methods are described in S.2.
385 The first experiments, also called HDDG experiments, were conducted in a darkroom using an HDDG and a fall height of 2 m. This setup was optimized for droplets with a diameter of 0.3 to 0.6 mm, by using a 300 mm lens with the resulting large magnification $M = 30.7$ px/mm. This led to a sampling area of $11.2 \times 8.4\,\mathrm{mm}^2$. The HDDG produced a localized drop jet, making it fairly easy to hit the sampling area. The height of the droplet fall is enough for the drops to reach more than 99% of the terminal velocity according to S.5. We used a 40 W
390 Light Emitting Diode (**LED**) ring purchased from a home supply store as a light source pointing upward and inward to achieve a high contrast between the bright drop edges and the dark background (see Fig. S3A).
The second experiment, also called the IVDG experiment, was carried out in the vertical tunnel of a spiral staircase using a IVDG as a droplet generator and a fall height of more than 10 m. With a smaller magnification

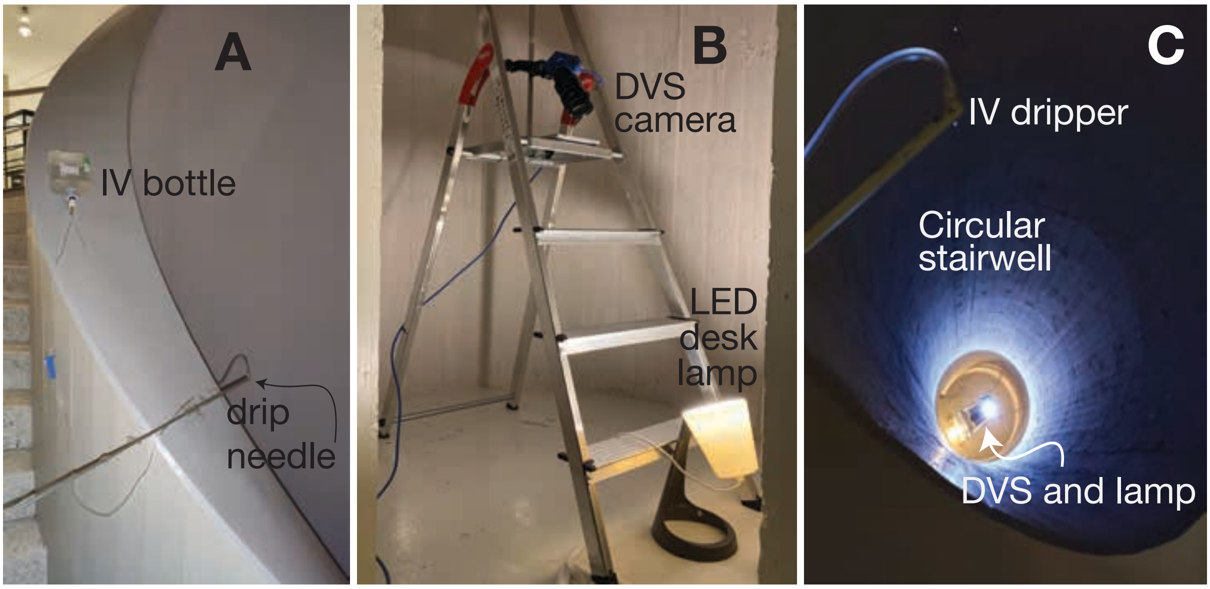

Figure S4: Pictures of the IVDG experimental setup. **A**: IVDG drop generator with water source and rod holding the needle. **B**: DVS camera and lighting setup. **C**: Tube inside the staircase with a fall height of 10 m with the DVS camera and lighting setup at the bottom.

of 7 px/mm (4.4× smaller than for the HDDG experiments), the magnification was reduced for droplets with a diameter of approximately 2.5 mm, while maintaining a relative precision similar to that of the HDDG setup. The main reason for this reduction in magnification was to more easily capture the droplets, which had a huge scatter compared to the HDDG scatter. With the IVDG, it was only possible to create a single droplet size because the droplet size is determined by the weight that breaks the surface tension with the needle. The higher magnification led to a larger sampling area of roughly $49 \times 37\,\mathrm{mm}^2$, which increases the chances to capture the larger drops, which have a much greater spread from the higher fall height needed to achieve a final speed close to the terminal speed. The height of the fall is sufficient for the drops to reach more than 97% of the terminal velocity according to S.5. The working space of the experiment IVDG was more limited (see Fig. S4B), so we used a single 5 W LED reading lamp to illuminate the drops from behind, which refracted the light towards the middle of the drop, leaving the edges dark. A large contrast was achieved between the bright background and the dark edges of the drop.

A key factor was the adjustable angle of the camera α (see Fig. 1B: left). The smaller is α, the more accurately the diameter can be measured and the larger is the sampling area, which leads to a faster estimate of Drop Size Distribution (**DSD**). Larger α's allow more precise velocity measurements, but smaller sampling area. The sampling area is the total area of the Plane of Focus (**PoF**) inside the field of view (**FoV**) multiplied by $\cos\alpha$. According to our findings, 20° to 30° was optimal for α.

Eq. (S6) was used for the diameter calculation. For the velocity calculation the non-simplified formula on the left side of (S7) was used for the HDDG experiment, while the simplified formula on the right side of (S7) was used for the IVDG experiment due to the negligible horizontal velocity component on the recording (see Fig. 1B: right).

Another important requirement was a flicker-free DC light source, which would otherwise create flicker artifacts in the recording. Pictures and illustrations of the experimental setups are provided in S.3.

S.4.1. Data selection

Each recording session collected data for a single droplet size. From the recording, we manually selected droplets that passed from the top to the bottom of the image and created a distinct hourglass shape. Fig. 1 illustrated how this procedure excluded droplets that did not pass through the PoF.

S.4.2. Error analysis

In both experiments, two aspects were considered to determine the propagation of the error of the measurements.

The first aspect is the combined measurement uncertainty of the DVSD and GT values which factors in all uncertainties. For example, one measurement uncertainty of the DVSD comes from the limited sensor resolution of the DVSD. Another one comes from the uncertainty of α. Together with other uncertainties, we could then calculate the combined standard uncertainty of the DVSD velocity and diameter measurements. The combined GT uncertainty consists of the uncertainty in height, droplet mass, drop creation frequency, etc. According to

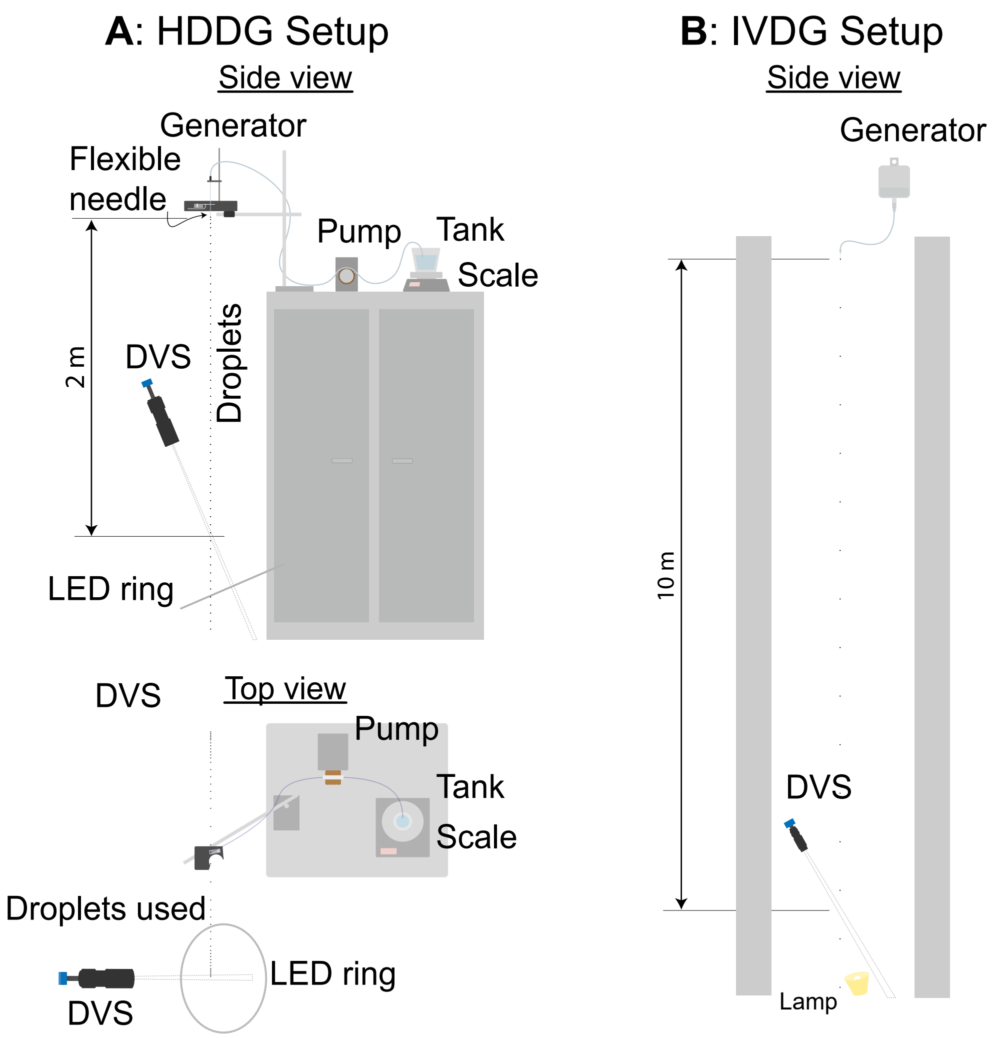

Figure S5: Illustration of experimental setups. A: HDDG setup is illustrated from a side view and a from a top view perspective. **B:** IVDG setup is illustrated from a side view perspective.

JCGM (2008), in the case of uncorrelated input quantities x_i, the combined standard uncertainty of a function $u(f)$ can be described as:

$$u(f) = \sqrt{\sum_{i=1}^{N} \left[\frac{\partial f}{\partial x_i} u(x_i)\right]^2} = \sqrt{\left[\frac{\partial f}{\partial x_1} u(x_1)\right]^2 + \left[\frac{\partial f}{\partial x_2} u(x_2)\right]^2 + \left[\frac{\partial f}{\partial x_3} u(x_3)\right]^2 + \dots} \tag{S1}$$

where $u(x_i)$ is the standard uncertainty of the input quantity x_i. The uncertainty is either derived with a *Type A evaluation*, where the standard uncertainty is evaluated with the experimental standard deviation from repeated observations, or with a *Type B evaluation*, where the estimated uncertainty is evaluated using our judgement of uncertainty. We used a *Type B evaluation*, either by using the manufacturer's instrument specifications or by a conservative estimate of the measured uncertainty. A linear approximation of the function is used for each input quantity. A spreadsheet in our online results folder[d] reports the final uncertainty values computed by our Matlab scripts.

The second aspect is accuracy, *i.e.*, comparison of the measured values from the DVS with the GT values. This is done by calculating the Mean Absolute Percentage Error (**MAPE**):

$$\text{MAPE} = \frac{100\%}{n} \sum_{i=1}^{n} \left| \frac{GT_i - ME_i}{GT_i} \right| \tag{S2}$$

[d] Results computations; see 00 README.txt

Setup parameters	Experiment	
	HDDG	IVDG
Drop diameter	0.3–0.6 mm	2.5 mm
Drop velocity	1.4–2.2 m/s	7.7 m/s
Fall height	2 m	10 m
Lighting	40 W LED ring	5 W LED bulb
Total luminance	4500 lm	470 lm
Location	darkroom	spiral staircase
Lens	TAIR-3 (Russian sniper rifle)	Edmund manual zoom
Listed focal length	300 mm	75 mm
Aperture ratio	f/4.5	f/1.2
Lens Spacer	M42-C (16 mm long)	-
# 5 mm C-CS lens spacers	23	2
Working distance	50 cm	50 cm
Sampling area	11×8 mm^2	49×32 mm^2
Camera FoV angle α	22°	29.5°
Magnification M	30.7 px/mm	7.0 px/mm

Table S1: Detailed setup parameters for the HDDG and IVDG experiment.

where GT_i is the GT value and ME_i is the measured value.

S.4.3. Optimizing the lighting

Water droplets refract light in the same way that convex glass elements do, namely towards the middle. This property of drops was used to determine a good lighting setup for DVS. To test this optical phenomenon, we took a dispensing needle and attached a tiny water drop at its end and took a photograph of it. We altered the distance between the circular light source until we were satisfied with the brightness of the drop edge. Fig. S6 shows the drop illumination for two different distances from the light source. In Fig. S6A the edges of the drop are clearly pronounced, whereas in Fig. S6A the edges are are very weak. It is therefore important to align the light source correctly, so that the edges of the droplet are well pronounced at the PoF. The light source used for this example was a ring light configuration with 6 LED bulbs. The light source used for the HDDG experiments was a ring light with a LED strip was used. However, the phenomenon is still the same. For the IVDG setup we used a single LED desk lamp.

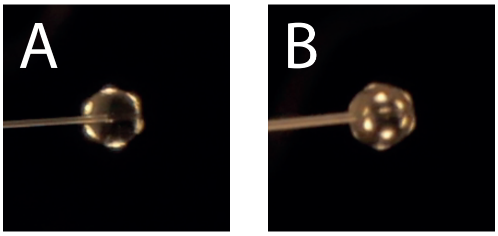

Figure S6: Drop illumination with **A** showing a drop with pronounced edges and **B** showing a drop with less pronounced edges.

S.4.4. Measurement of camera angle α

The camera angle α was measured by aligning an iPhone Xs flush with the back of the DVS body and reading off its 3D-orientation from the Inertial Measurement Unit (**IMU**) accelerometer (using the Apple bubble level app). Before the measurement, we verified that the angle read zero when the phone was held on a flat surface.

S.4.5. Measurement of fall height

The fall height between the IVDG and the DVS sampling area was measured using a long wire, and the fall height between the HDDG and the DVS sampling area was measured using a 2 m folding ruler.

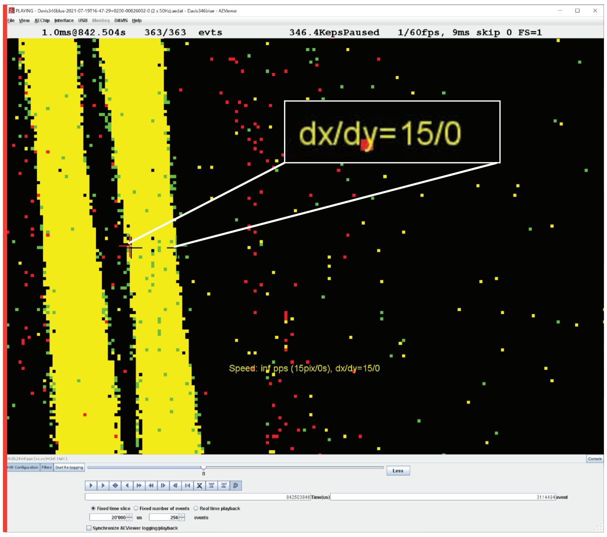

Figure S7: Measurement of the diameter from the DVS recording using jAER. Two droplets passed during the accumulation time. After marking the left and right sides of the hourglass waist, *Speedometer* displays the diameter d_r [px]. This is a sample recording of an HDDG drop with a drop creation frequency f of 100 Hz (2×50 Hz, two-sided).

S.4.6. Image plane droplet diameter and velocity measurement from DVS recording

The droplet diameter and velocity are measured from the DVS recording with jAER (`https://jaerproject.net`). The *Speedometer* [e] plugin filter allows for convenient measurement of the diameter and velocity by outputting the velocity seen on the recording v_r [kpx/s], horizontal displacement Δx_r [px] and vertical displacement Δy_r [px].

An hourglass appears on a DVS recording after accumulating all events from one droplet passing through the FoV. The width at the center of the hourglass indicates the diameter of that water drop when in focus (see Fig. 1C on the right). This width d_r [px] is measured with *Speedometer* using two mouse clicks. A sample recording of a HDDG drop with a drop creation frequency f of 100 Hz (2×50 Hz, two-sided) is analyzed. Two drops are visible, but only the second drop on the right side is analyzed.

Fig. S7 shows the diameter measurement. The right point at the thinnest width of the *hourglass* is selected first (see Fig. S7A). Next the left point on the thinnest width of *hourglass* is selected (see Fig. S7B). *Speedometer* displays the diameter of the recording $d_r = 15$ px. The diameter d [mm] can then be calculated with (S6).

Fig. S8 shows the velocity measurement. Before the drop reaches the PoF (smallest diameter), the midpoint of the drop is selected (see Fig. S8A). After that, the midpoint of the drop is selected again after the drop has passed the PoF (see Fig. S8B). This is done by scrubbing through the recording. The *Speedometer* outputs the velocity of the droplet in the image $v_r = 20.8$ kpx/s. The physical velocity v can then be calculated directly with Eq. (S7) (right side). For a more accurate calculation, the time difference $\Delta t = 5304$ µs can be used together with the horizontal and vertical displacement $\Delta x_r = 10$ px and $\Delta y_r = 110$ px to calculate the velocity v according to (S7) (left side).

Calculations for diameter d [mm] and velocity v [m/s] are described in S.4.10.

S.4.7. Optical and geometrical calibration

Before the diameter and velocity measurement with the DVS can be performed, the camera geometry and optics must first be calibrated. First, the *camera angle* α, which is the angle between the Line of Sight (**LoS**) of the camera and the vertical yz-plane (see Fig. 1B: left), is measured using a smartphone accelerometer (see S.4.4). The *droplet angle* β is the angle between the projected droplet trajectory (trajectory in camera image) and the camera image y_r-axis on the DVS recording (see Fig. 1B: right). The magnification M describes how large a certain distance in reality on the PoF would appear on the DVS recording and vice versa. The magnification calibration is done by recording a miniature checkerboard calibration chart held at the PoF with the DVS. The magnification M is measured by dividing the checkerboard square size in mm by the number of pixels.

S.4.8. Field of view

The geometry of the FoV and Angle of View (**AoV**) is important for measuring the velocity on the DVS camera. The illustration is can be seen in Fig. S9. The AoV θ is an important quantity, which can be calculated with the working distance w, horizontal FoV F_x and vertical FoV F_y, that are both defined at the PoF. This is done as follows:

$$\theta_i = 2 \arctan\left(\frac{F_i}{2w}\right) \tag{S3}$$

[e] Speedometer class. Speedometer usage.

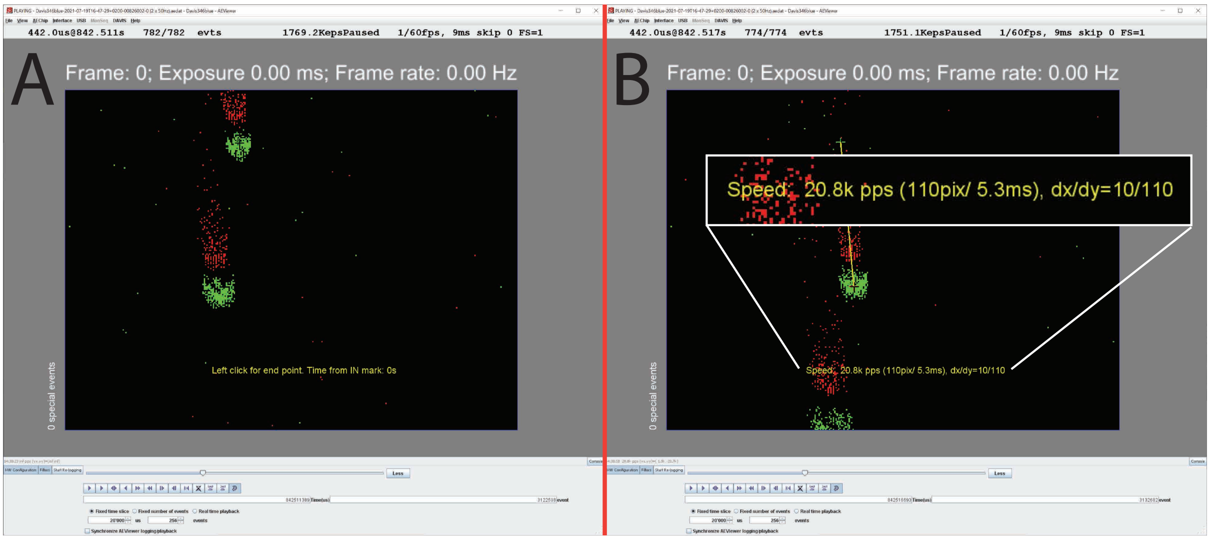

Figure S8: Measurement of the velocity from the DVS recording using jAER. **A**: Mark IN point first on the mid-point of the right drop before the drop passes the PoF. **B**: Mark OUT point on the mid-point of the drop after the right drop passes the PoF and *Speedometer* outputs the velocity v_r [kpx/s]. This is a sample recording of an HDDG drop with a drop creation frequency f of 100 Hz (2×50 Hz, two-sided).

where F_i is calculated with the magnification M and number of pixels in the according pixel direction of the DVS:

$$\begin{aligned} F_\mathrm{x} &= \frac{346\ [\mathrm{px}]}{M} \\ F_\mathrm{y} &= \frac{260\ [\mathrm{px}]}{M} \end{aligned} \tag{S4}$$

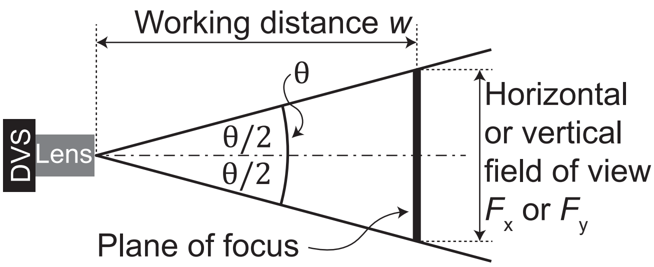

Figure S9: Illustration of the FoV F_x and F_y of the camera including the corresponding AoV θ_x and θ_y.

Table S2 shows the AoV θ_x and θ_y for the HDDG and IVDG setup. Due to the small values, an assumption of a parallel FoV is appropriate ($\theta_i = 0$). The magnification M in the vicinity of the PoF can be assumed to be constant, which simplifies the velocity calculation.

Angles of view

Experiment	θ_x [°]	θ_y [°]
HDDG	1.3	1.0
IVDG	5.7	4.3

Table S2: AoV θ_x and θ_y for the HDDG and IVDG experiment in horizontal and vertical direction (x- and y-direction).

S.4.9. Depth of Field

The Depth of Field (**DoF**) is approximately given by (S5):

$$\mathrm{DoF} = \frac{2w^2Nc}{f^2} \tag{S5}$$

for a given circle of confusion c, focal length f, f-number N, and working distance w (Allen and Triantaphillidou 2012). N is the ratio of f to the diameter of the entrance pupil. c is the diameter of the largest image plane circle that is indistinguishable from a point.

Using the DVS pixel pitch of 18.5 um for c, $w = 50$cm, $N = 4.5$, and $f = 300$mm for the HDDG measurements results in $\mathrm{DoF} = 0.46$mm.

A smaller DoF results in a more pronounced hourglass shape for the accumulated DVS events produced by a droplet. (S5) shows that we can minimize the DoF by using a fast lens (small N) and by maximizing the ratio of focal length to working distance (f/w).

S.4.10. Droplet diameter and velocity computation from DVS image plane measurement

Given the image plane droplet diameter d_r (Sec. S.4.6), the droplet diameter d can be calculated from (S6):

$$d\ [\mathrm{mm}] = \frac{d_\mathrm{r}\ [\mathrm{px}]}{M\ [\mathrm{px/mm}]}. \tag{S6}$$

For droplet velocity measurement, it is useful to use a lens with a long focal length, resulting in a small AoV θ_i, so that the magnification M at the PoF can be assumed to be constant. To further mitigate this effect, it is important to measure the velocity as close as possible to the center of the hourglass. The velocity is also measured with the *Speedometer* tool. During playback of a droplet, the velocity is measured by clicking the middle of the droplet at two points surrounding the passage of the droplet through the PoF, resulting in the *Speedometer* outputting the horizontal and vertical displacement Δx_r and Δy_r as well as the time difference Δt and the velocity vector v_r [kpx/s] in px/s. The droplet fall velocity is calculated from (S7):

$$v\ [\mathrm{m/s}] = \frac{\sqrt{(\Delta x_\mathrm{r}\ [\mathrm{px}])^2 + \left(\frac{\Delta y_\mathrm{r}\ [\mathrm{px}]}{\sin\alpha}\right)^2}}{10^3 \cdot \Delta t\ [\mathrm{s}] \cdot M\ [\mathrm{px/mm}]} \overset{(*)}{\approx} \frac{\Delta y_\mathrm{r}\ [\mathrm{px}]}{10^3 \cdot \sin(\alpha) \cdot \Delta t\ [\mathrm{s}] \cdot M\ [\mathrm{px/mm}]} = \frac{v_\mathrm{r}\ [\mathrm{kpx/s}]}{\sin(\alpha) \cdot M\ [\mathrm{px/mm}]} \tag{S7}$$

(S7) is simplified to the second form when β is small and therefore $(*)$ $\Delta y_\mathrm{r} \gg \Delta x_\mathrm{r}$. This simplified formula can only be applied if the drop trajectory is parallel to the vertical yz-plane (see Fig. 1B: left and Fig. S5: bottom left corner) for a correct velocity calculation, otherwise, α, which is used for the velocity simulation, would not be constant anymore. Fig. 1C shows an abstract illustration of a measurement of diameter and velocity from a DVS recording, where the black circles show where the actual droplets are. The circles enclose the bottom edge of the ON events (green points) and OFF events (red points). The tracking points of the droplets that we used for the DVS velocity estimates are the centers of the black circles. Sec. S.4.6 shows examples of our actual jAER measurements of diameter and velocity.

S.4.11. Ground truth droplet size measurement

Our HDDG droplets were larger than the 100 µm droplets which were the focus of Kosch and Ashgriz (2015). The needle frequency is adjusted with a function generator and resulted in droplet diameters between 0.3 and 0.6 mm, which in our case corresponded to a droplet creation frequency between 60 and 220 Hz and flow rate 5.19×10^{-3} g/s. At An ISMATEC REGLO Digital peristaltic pump supplied our HDDG with water at constant flow rate from a tank placed on top of a KERN 440 weighing scale. The scale measured how much water left the tank over time to determine the flow rate. By assuming spherical water drops, their diameter is inferred from their mass, which increases with flow rate but decreases with drop creation frequency. The drop creation frequency describes how many drops per second are produced. According to a water droplet model proposed by Beard and Chuang (1987), a spherical assumption is very accurate for submillimeter drops.

For the IVDG experiments (described in S.4), the mass of single droplets was determined with a scale (detailed description in S.4.12). For these droplets, the model by Beard and Chuang (1987) predicts a slight average drop deformation due to drag. However, this average deformation is 0.8% in the case of 2.50 mm droplets, making them appear to be 2.52 mm when viewed from roughly 30°. The average deformation thus introduced only a very small systematic DVS error. A random error was additionally introduced from the vibration of the 2.5 mm droplets.

The calculation of the diameter from mass with a spherical assumption is described in S.4.12 for the HDDG and IVDG. These diameter calculations served as our GT values to evaluate the performance of our DVS diameter measurements.

S.4.12. Ground truth droplet diameter from mass

We used an electronic weighing scale with 0.1mg precision to measure the decrease in mass Δm of the water tank over a certain period of time Δt. The volumetric flow rate $\dot{V}$ is calculated as (S9):

$$\dot{V} = \frac{\Delta m}{\rho \Delta t} \tag{S8}$$

where ρ is the density of water. With the flow rate $\dot{V}$ and the assumption of a sphere, the diameter is calculated as (S9):

$$d = \left(\frac{6\dot{V}}{\pi f}\right)^{1/3} \tag{S9}$$

where f is the drop creation frequency.

To create larger droplets, we used the IVDG. To determine the mass of a single droplet, many droplets were counted and collected in a reservoir positioned on the scale while the total mass m_{tot} and the number of drops N were recorded. The volume of a single drop is calculated as

$$V_{\text{drop}} = \frac{m_{\text{tot}}}{\rho N} \tag{S10}$$

The diameter can then be calculated as

$$d = \left(\frac{6V_{\text{drop}}}{\pi}\right)^{1/3} \tag{S11}$$

where the drop is assumed to be a sphere. The diameters calculated from (S9) and (S11) are used as GT values to compare with the diameter measurements of DVS.

S.5. Numerical speed simulation of falling drops

A numerical velocity simulation was used to analyze the dynamic behavior of a falling droplet with a diameter up to 2.5 mm. We used the results of the simulation to determine the terminal speed and the fall height needed to reach any desired final speed, ideally close to the terminal speed. Being close to the terminal speed ensures that DVS captures drops with properties similar to real rainfall, and ensures that an uncertainty in height measurement leads to a small deviation from the predicted velocity by simulation.

For simulation, all water drops were assumed to be solid and smooth spheres, which is an eligible approximation especially for drops less than 1 mm that do not experience any significant deformation according to Beard and Chuang (1987) and Van Boxel et al. (1997). Any effect of deformation or vibration due to air drag and turbulence was neglected. Literature values for the air and water properties were used, where the air and water temperatures for 20 and 25°C were interpolated to 22.5°C.

The differential equation for the velocity simulation consists of a drag force, gravity, and acceleration term. The differential equation is numerically solved using the Euler forward method. The relation between drag coefficient and Reynolds number for solid spheres is used, which was fitted to the model of Yang et al. (2015) with the empirically obtained data of Brown and Lawler (2003).

Numerical velocity simulation is used as the velocity GT to compare velocity measurements with DVS. To determine the accuracy of the simulation, the terminal velocity of the simulation is compared with the accepted reference data of Gunn and Kinzer (1949). The results show that they are very close to each other for drops up to 1 mm. However, for larger drops, the simulation predicts slightly higher velocities; for the 2.5 mm drops created with the IVDG, the simulation predicts 7.9 m/s whereas Gunn and Kinzer (1949) predict 7.5 m/s.

Fig. S10A plots the model for different drop diameters. For larger droplets, the fall height must be higher to reach the terminal velocity. Moreover, the terminal velocity for larger drops is larger than for smaller ones. Fig. S10B compares the simulated velocity and the measured data from Gunn and Kinzer (1949). The simulation starts to differ from the data for droplets with a diameter above 1.5 mm.

According to our simulation, a fall height of 2 m is sufficient for drops with a diameter of up to 0.6 mm to reach 99% of the terminal velocity, while for 2.5 mm drops, a fall height of 10 m is necessary to reach 97% of the terminal velocity (see Fig. S10). Thus, a fall height of 2 m was used for the HDDG experiment and 10 m was used for the IVDG experiment.

S.5.1. Details of droplet speed simulation

This following describes the details of the model used to simulate the speed of a falling water droplet. The goal is to find the velocity v of the drop as a function of the vertical distance y the drop has traveled from its initial position for any given diameter d. This model allows us to determine the terminal speed and the required fall height to reach a certain fraction of the terminal speed v_{term}, ideally close to the terminal speed. Our model is based on Yang et al. (2015).

The drag force F_{D} acts on a falling water drop that eventually reaches equilibrium at terminal velocity v_{term} with the gravitational force mg. The drag force is defined as (S12):

$$F_{\text{D}} = \frac{1}{2}\rho_{\text{air}} c_{\text{D}}(Re) A v^2 = k(Re) v^2 \tag{S12}$$

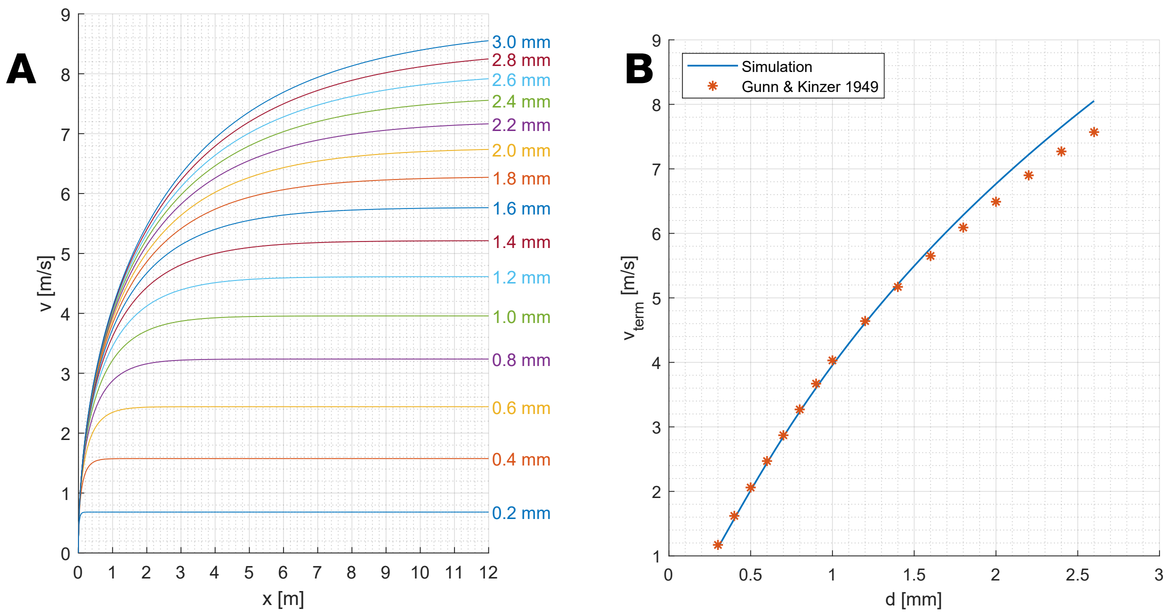

Figure S10: Falling droplet simulation results. **A:** Velocity simulation for a fall height up to 12 m and for different drop diameters (written on the right side); vertical displacement y vs. velocity v. Literature values for the density of air ρ_{air}, kinematic viscosity of air ν_{air} and density of water ρ_{water} were used for a temperature of 20°C. **B:** Comparison of the terminal simulated terminal velocity to the data of Gunn and Kinzer (1949); diameter d vs. terminal velocity v_{term}. Literature values for the density of air ρ_{air}, kinematic viscosity of air ν_{air} and density of water ρ_{water} were used for a temperature of 20°C.

where c_{D} is the drag coefficient depending on the Reynolds number Re, ρ_{air} is the density of air, A is the area facing the fluid (for spheres: $A = \pi(\frac{d}{2})^2$) and $k = \frac{1}{2}\rho_{\text{air}} c_{\text{D}} A$. The equation of motion can be derived as (S13):

$$ma = mg - F_{\text{D}} = mg - k(Re)v^2 \tag{S13}$$

595 where a is the acceleration, v is the velocity, and g is the gravitational acceleration. (S13) can be rewritten as a differential equation:

$$m\ddot{y} = mg - k(Re)\dot{y}^2 \tag{S14}$$

where y describes the vertical displacement of the droplet from the droplet generator. As mentioned above, the drag coefficient c_{D} depends on the Reynolds number Re. The curve fit for the drag coefficient derived by Yang et al. (2015) is used for the simulation, which is expressed as (S15):

$$\begin{aligned} x &= \frac{\ln(1 + Re)}{10} \\ \alpha &= \left[1 - \exp\left(-3.24x^2 + 8x^4 - 6.5x^5\right)\right] \cdot \frac{\pi}{2} \\ c_{\text{D}} &= \frac{24}{Re} \cdot \left(1 + \frac{3}{16}Re\right)^{0.635} \cdot \cos^3\alpha + 0.468 \cdot \sin^2\alpha \end{aligned} \tag{S15}$$

600 where the Reynolds number Re is defined as

$$Re = \frac{\rho v L}{\mu} = \frac{vL}{\nu}, \tag{S16}$$

where ρ is the density of the fluid, v is the flow velocity, L is the characteristic length (in this case $L = d$), μ is the dynamic viscosity of the fluid, and ν is the kinematic viscosity of the fluid. (S15) is a very good approximation for Reynolds numbers $Re < 2 \times 10^5$, which water drops never exceed, according to Gunn and Kinzer (1949).

MATLAB code to compute discrete time updates of these equations is available from our cloud drive (see
605 Sec. 5).

References

Allen, Elizabeth and Sophie Triantaphillidou (Nov. 2012). *The Manual of Photography*. CRC Press. ISBN: 9781136091100. URL: https://play.google.com/store/books/details?id=h4LOAwAAQBAJ.

Beard, Kenneth V and Catherine Chuang (1987). "A new model for the equilibrium shape of raindrops". In: *Journal of Atmospheric Sciences* 44.11, pp. 1509–1524. DOI: 10.1175/1520-0469(1987)044<1509:ANMFTE>2.0.CO;2.

Brandli, C et al. (Oct. 2014). "A 240x180 130 dB 3 us Latency Global Shutter Spatiotemporal Vision Sensor". In: *IEEE J. Solid-State Circuits* 49.10, pp. 2333–2341. ISSN: 0018-9200, 1558-173X. DOI: 10.1109/JSSC.2014.2342715.

Brown, Phillip P and Desmond F Lawler (2003). "Sphere drag and settling velocity revisited". In: *Journal of environmental engineering* 129.3, pp. 222–231. DOI: 10.1061/(ASCE)0733-9372(2003)129:3(222).

Gunn, Ross and Gilbert D Kinzer (1949). "The terminal velocity of fall for water droplets in stagnant air". In: *Journal of Atmospheric Sciences* 6.4, pp. 243–248. DOI: 10.1175/1520-0469(1949)006<0243:TTVOFF>2.0.CO;2.

JCGM (2008). *Guide to the Expression of Uncertainty in Measurement - JCGM 100:2008*. Working Group 1 of the Joint Committee for Guides in Metrology (JCGM/WG 1).

Kosch, Sebastian and Nasser Ashgriz (Apr. 2015). "Note: A simple vibrating orifice monodisperse droplet generator using a hard drive actuator arm". In: *Rev. Sci. Instrum.* 86.4, p. 046101. ISSN: 0034-6748, 1089-7623. DOI: 10.1063/1.4916703.

Lichtsteiner, Patrick, Christoph Posch, and Tobi Delbruck (Feb. 2008). "A 128×128 120 dB 15 μs latency asynchronous temporal contrast vision sensor". In: *IEEE J. Solid-State Circuits* 43.2, pp. 566–576. ISSN: 0018-9200, 1558-173X. DOI: 10.1109/jssc.2007.914337.

Taverni, G et al. (May 2018). "Front and Back Illuminated Dynamic and Active Pixel Vision Sensors Comparison". In: *IEEE Trans. Circuits Syst. Express Briefs* 65.5, pp. 677–681. ISSN: 1558-3791. DOI: 10.1109/TCSII.2018.2824899.

Van Boxel, John H et al. (1997). "Numerical model for the fall speed of rain drops in a rain fall simulator". In: *Workshop on wind and water erosion*. dare.uva.nl, pp. 77–85. URL: https://dare.uva.nl/document/2/171269.

Yang, Hongli et al. (2015). "General formulas for drag coefficient and settling velocity of sphere based on theoretical law". In: *International Journal of Mining Science and Technology* 25.2, pp. 219–223. DOI: 10.1016/j.ijmst.2015.02.009.